

Hexagonal Single Crystals of Perylene with Patterned Heterogeneous Domains

Ken Takazawa^{a,*} and Jun-ichi Inoue^b

^aResearch Center for Electronic and Optical Materials, National Institute for Materials Science, Tsukuba, Ibaraki 305-0003, Japan

E-mail: takazawa.ken@nims.go.jp

^bResearch Center for Electronic and Optical Materials, National Institute for Materials Science, Tsukuba, Ibaraki 305-0044, Japan

Keywords

Polymorphism; Perylene crystal; Fluorescence microscopy; Ultralow-frequency Raman microscopy; Crystal quality.

Abstract

Hexagonal single crystals of perylene were grown on a substrate by solution evaporation. Fluorescence microscopy images showed patterned heterogeneous domains with different fluorescence colors. Polarized ultra-low-frequency Raman microscopy revealed that the crystal structure is homogeneous throughout the entire crystal despite the domains observed in the fluorescence images. We concluded that hexagonal crystals were formed by the further growth of the rhombic β -crystal, which is one of the two polymorphs of the perylene crystal. This mechanism explains the formation of domains with different crystal

qualities, resulting in different fluorescence colors.

Introduction

Organic crystalline materials have attracted considerable attention in various fields, including electronics, photonics, catalysis, and energy storage, because they possess unique and promising properties compared to their inorganic counterparts [1–4]. The properties of organic crystals are closely related to their sizes, shapes, and internal molecular arrangements (crystal structures). Therefore, controlling these parameters is crucial for synthesizing crystals with desired functionalities. To this end, considerable effort has been made for the controlled synthesis using both solution- and vapor-phase crystal growth techniques.

Solvent evaporation on a surface is a facile technique widely used to synthesize organic crystals with well-defined shapes. In this method, a solution of molecules is deposited on a surface and allowed to evaporate, leading to the precipitation of crystals on the surface after the solvent has completely evaporated. Although this technique is advantageous in terms of simplicity, it sometimes suffers from poor reproducibility. The crystallization of the evaporating solution on the surface involves dynamic processes such as surface dewetting, thinning of the solution film, and solution flow, which are further influenced by various factors such as solvent, concentration, temperature, humidity, and surface properties. Owing to the many factors involved, small differences in them result in precipitation of crystals with different morphologies and crystal structures [5–7]. Conversely, sensitivity to these factors indicates that elaborate tuning and control can yield crystals with new morphologies and crystal structures, which can lead to new functionalities.

In this study, we tested the feasibility of this concept using perylene, a polyaromatic hydrocarbon (PAH) consisting of four benzene rings. Perylene and its

substituted compounds have vast potential for applications in organic semiconductors, such as field-effect transistors and light-emitting diodes [8–13]. As such, the optical and electronic properties of their single crystals have been studied extensively. Perylene crystals have two polymorphic forms with distinct shapes and fluorescence colors [14–16]. Thermodynamically stable α -crystals have a square or rectangular shape and emit orange fluorescence, whereas metastable β -crystals have a rhombic shape and emit green fluorescence [17–19]. The difference in fluorescence color is attributed to the difference in crystal structure, which governs the exciton properties of the crystals [20–26]. Both solution- and vapor-phase crystal growth processes under ambient conditions yield stable α -crystals as major products, although the selective growth of metastable β -crystals has also been reported [17–19].

Because of these morphological and polymorphic features, perylene is a suitable molecule for feasibility testing. We attempted to obtain single crystals of perylene with a new morphology (other than square and rhombic) and crystal structure via solvent evaporation by tuning and controlling the conditions influencing the crystallization process. We demonstrated that hexagonal single crystals of perylene can be efficiently grown under certain conditions. Hexagonal crystals of optically active molecules are of particular interest because they can hold whispering-gallery modes, resulting in crystals functioning as optical cavities [27]. Moreover, we found that the hexagonal crystals had patterned heterogeneous domains with different fluorescence colors. To investigate the crystal structures of these domains, the lattice (intermolecular) vibrational modes of each domain were observed using polarized ultralow-frequency (ULF) Raman microscopy, which revealed that these domains have different crystal qualities. Based on Raman and fluorescence microscopy investigations, we propose that hexagonal crystals are formed

by a process in which two different crystal growth modes occur repeatedly as the solvent evaporates. These results indicate that solution evaporation under tuned and controlled conditions can induce unique crystallization processes that do not occur in bulk solutions. Therefore, our approach is promising as a technique for synthesizing organic crystals with new functionalities.

Experimental Section

Sample preparation: Perylene (molecular weight: 252.31; chemical structure: Figure 1a) was purchased from Wako Pure Chemical Industries and used as received. A 10 mM toluene solution of perylene was prepared by sonication. A microscope cover glass (18 mm × 18 mm, Matsunami Glass Ind.) was used as the substrate without further cleaning. Approximately 10 μ L of the sample solution was dropped onto the substrate, and the solvent was allowed to evaporate. For precise control of the conditions, we conducted this procedure in a glove box with dry nitrogen gas flow at a temperature of \sim 23 $^{\circ}$ C. Note that the surface properties of the substrate strongly influenced the crystallization process in our method, and the conditions described in this section were optimized for the cover glass used. Therefore, the use of cover glasses from other brands may require re-optimization of the conditions.

Fluorescence microscope imaging: An epi-illumination fluorescence microscope (BX-51, Olympus) was used. The set of interference filters for fluorescence microscopy consisted of a bandpass filter (Omega Optical, XF1076, pass band: 385–415 nm), a dichroic mirror (Omega Optical, XF2040), and a long pass filter (Omega Optical, XF3088, pass band: > 435 nm). Fluorescence images were recorded using a color charge-coupled device (CCD)

camera (Jenoptic, ProgRes C10).

Spatially resolved fluorescence microscopy: The output of a continuous-wave diode laser (Lasos, $\lambda = 405$ nm) was coupled to a microscope (Olympus, BX-51) and directed to the sample using a dichroic mirror. The laser beam was focused onto the sample using a 100 \times objective lens (spot size: ~ 400 nm). The fluorescence from the sample was collected using the same objective lens. One end of the optical fiber was placed on the image plane of the microscope to selectively couple the fluorescence (spatial resolution: ~ 4 μm) to a spectrometer (Ocean Optics, USB400). The spectral intensity was calibrated using an NIST-traceable halogen lamp (Ocean Optics, HL-3P-CAL).

Ultralow-frequency Raman microscopy: The output of a continuous-wave diode laser (Necsel, $\lambda = 785$ nm) was used for the excitation. The laser beam was consecutively reflected by two volume Bragg gratings (VBGs, OptiGrate, BP-785), which function as ultra-narrow laser line filters (bandwidth: ~ 5 cm^{-1}), passed through a polarizer and introduced into the microscope (Olympus, BX-51). The laser was then directed to the sample using a half mirror (Thorlabs, BSW26R) and focused on the sample using a 100 \times objective lens (spot size: ~ 1 μm). Scattering from the sample was collected with the same objective lens, extracted from the microscope using a mirror, and passed through two VBGs (OptiGrate, BNF-785-OD4-11M), which reflected (blocked) residual laser light (bandwidth: ~ 5 cm^{-1}). Spectra were recorded using a CCD camera (Princeton Instruments) attached to a monochromator (Acton Research, SpectraPro 2150, 1200 g/mm grating).

Results and Discussion

First, we briefly describe the optical properties and crystal structures of the α - and β -crystals of perylene. Figures 1b and 1c show the fluorescence microscopy images of the α - and β -crystals, respectively, prepared using our solution evaporation method. The yields of these crystals are described later. The α -crystal has a square shape with orange fluorescence, whereas the β -crystal has a rhombic shape with green fluorescence. For both crystals, the fluorescence intensities are concentrated at the crystal edges. This is attributed to the waveguiding effect; the fluorescence generated by optical excitation is guided within the crystals by total internal reflection at the upper and lower surfaces of the crystals and is emitted from the crystal edges [28, 29].

The orange curve in Figure 1d shows the spatially resolved fluorescence spectrum of the α -crystal measured at its central position. The α -crystal exhibited a broad band peaking at ~ 610 nm with a long-wavelength tail extending to ~ 750 nm. Nishimura et al. measured the fluorescence spectrum of a high-quality α -crystal grown via vacuum sublimation and observed a free exciton (FE) peak at 480 nm and a broad self-trapped exciton (STE) band on the long wavelength side of the FE peak [23]. Based on their assignment, the broad band observed in our spectrum was assigned to STE emissions (marked as STE). The absence of the FE peak indicates that the quality of our crystal is lower than that of their crystals [23]. The green curve in Figure 1d shows the spatially resolved fluorescence spectrum of the β -crystal measured at its central position. The β -crystal displays a broad band peaking at ~ 600 nm with a long-wavelength tail up to ~ 720 nm. The spectrum on the short-wavelength side of the broad peak exhibits a few shoulders. The fluorescence spectrum of a high-quality β -crystal grown by vacuum sublimation shows an FE peak at 483 nm and a broad STE band with resolved vibrational progression [23]. The positions of these peaks observed for the high-quality crystals are consistent

with those of the shoulders observed in the spectrum. Therefore, the shoulder at $\lambda \approx 487$ nm was assigned to the FE band (marked as FE), whereas the others were assigned to the vibrational progression of STE.

The fluorescence spectra of the α - and β -crystals with different intensity profiles from those of our spectra have been reported by several authors [17, 19, 21, 22, 30]. In these spectra, the intensities in the short-wavelength range ($\lambda < \sim 580$ nm) drop more rapidly to zero compared to our spectra for both the α - and β -crystals. This difference is attributed to the waveguiding effect. As shown in Figures 1b and 1c, the fluorescence intensity of the crystals was mostly concentrated at their edges. Therefore, the spectra measured by collecting the fluorescence from the entire crystal without spatial resolution were mainly contributed by edge fluorescence, which is emitted from the crystals after it propagates within the crystals for certain distances via the waveguiding effect. During propagation, the short-wavelength side of the fluorescence, which overlaps with the long-wavelength tail of the absorption band, is reabsorbed by the crystal, and its intensity is reduced [28]. By contrast, our spatially resolved spectra were obtained by collecting the fluorescence emitted directly from the excitation laser spot. Therefore, the spectra were not affected by reabsorption. The absence of reabsorption is the origin of the difference between our spectra and the previously reported spectra. To confirm this, we measured the spectra of the α - and β -crystals by collecting fluorescence from the entire crystal (Figure S1). The spectra show intensity profiles similar to those previously reported. Owing to the reduced intensity in the short-wavelength range, the shoulders observed for the β -crystal were not observed in the spectrum.

The shapes and structures of the α - and β -crystals are schematically illustrated in Figures 1e and 1f, respectively. Both the crystals belong to the space group of $P2_1/c$.

The α -crystal contains four molecules in the unit cell, which form two pairs of dimers. The dimers stack in a herringbone manner, with the stacking direction parallel to the b-axis [16, 31]. The β -crystal consists of two molecules in a unit cell with a standard herringbone-stacking structure with the stacking direction parallel to the b-axis [16, 31].

Figure 2a shows an optical micrograph of typical hexagonal crystals prepared using our method. Under the sample preparation conditions described in the Experimental Section, approximately 80% of the crystals had a hexagonal shape, while most of the rest were square-shaped α -crystals. The percentage of rhombic β -crystals grown was less than one. The side lengths of the hexagonal crystals were typically 30–60 μm . Figure 2b shows a side view of a hexagonal crystal aligned nearly vertically to the surface using a micromanipulator [32]. The crystal thickness was approximately 5 μm . A polarized optical microscope image of the hexagonal crystals exhibited a uniform color, indicating that no inhomogeneities in the crystal structure or thickness were detectable with the polarized microscope (Figure 2c). However, fluorescence microscopy images of the hexagonal crystals exhibited strong inhomogeneity (Figure 2d). The image shows that the crystal consists of two triangular domains with orange fluorescence, hereafter referred to as the orange domains. Areas other than the orange domains emit green/yellow fluorescence, referred to as green domains.

Figure 2e shows a high-magnification fluorescence microscopy image of a hexagonal crystal. The orange domains were located symmetrically with respect to the axis parallel to one of the diagonal axes of the hexagon. We refer to this symmetric axis as the s-axis (Figure 3e). Dark stripes nearly parallel to the s-axis were observed in the orange domains, and the boundaries between the orange and green domains were not smooth, but irregularly bent. In addition, a rhombic-shaped area, slightly darker than the

other green domains, was observed between the orange domains. These features are commonly observed in distorted and elongated hexagonal crystals (Figure 2f–2h).

To investigate the origin of these patterned heterogeneous domains, we first measured the spatially resolved fluorescence spectra of both orange and green domains (Figure 3). The spectra of both domains show shoulders at the same positions as those observed for the β -crystal, suggesting their crystal structure is similar to that of the β -crystal. The spectra shown in Figure 3 were normalized to the intensity of the FE peak to clarify the spectral differences between the green and orange domains. Although the intensity distribution of the green domain spectrum was nearly identical to that of the β -crystal, the orange domain exhibited a significantly stronger intensity in the STE band region (550–750 nm) than that of the β -crystal.

We observed the lattice (intermolecular) vibrational modes of both domains using polarized ultralow-frequency (ULF) Raman microscopy to further investigate the crystal structures of the green and orange domains. As the lattice vibration modes of organic crystals are sensitive to their crystal structures, ULF Raman spectroscopy is a suitable technique for identifying crystal structures. First, we observed the lattice vibration modes of the α - and β -crystals for reference purposes. Figure 4a shows the polarized ULF Raman spectrum of the α -crystal oriented such that the b-axis is horizontal in the image plane (inset in Figure 4a). The excitation laser was polarized perpendicularly to the b-axis (red arrow in the inset of Figure 4a). The spectrum showed four peaks at 32, 48, 76, and 100 cm^{-1} in the ULF region below 200 cm^{-1} . Figures 4b and 4c show the ULF Raman spectra of the β -crystal oriented such that the b-axis was horizontal in the image plane. The spectrum measured with the laser polarized parallel to the b-axis exhibited a single peak at 110 cm^{-1} , whereas that measured with the perpendicular polarization

exhibited three peaks at 59, 85, and 110 cm^{-1} .

The Raman active lattice vibrations of many PAH crystals are approximated by librations, which are rotational motions (torsional vibrations) around the three principal axes of inertia for each molecule [33–35]. When the unit cell consists of more than one molecule, the three modes associated with each principal axis are further split into multiple levels by coupling with the same modes of the other molecules in the unit cell. Koscic et al. reported that the Raman active lattice vibrations of α - and β -crystals can be classified as librations and provided estimated frequencies based on a libration model [35]; these frequencies were consistent with our spectra. A detailed assignment on the Raman spectra will be presented in future studies. Aside from the detailed assignments, our polarized ULF Raman spectra indicate the following: (i) α - and β -crystals can be clearly identified from the spectra, and (ii) the direction of the crystal axis can be determined from the polarization dependence of the spectra. Based on these facts, we investigated the crystal structure of hexagonal crystals.

The hexagonal crystal was oriented such that the s-axis was oriented horizontally in the image plane (inset Figure 4d). The polarized ULF Raman spectra of the green domain were measured with the laser polarized parallel (Figure 4d) and perpendicular (Figure 4e) to the s-axis. These spectra agree with those of the β -crystal (Figures 4b and 4c): the excitation with the horizontally polarized laser resulted in a single Raman peak at 110 cm^{-1} , while the one with the vertically polarized laser resulted in three peaks at 59, 85, and 110 cm^{-1} , thus confirming that the green domain has the same crystal structure as the β -crystal, and its b-axis is parallel to the s-axis. We measured the Raman spectra of the orange domains in the same hexagonal crystal (Figures 4f and 4g). Despite the difference in fluorescence color, the orange domain exhibited the same spectra and

polarization dependence as the β -crystal. Based on these results, we can conclude that the hexagonal crystal, including both the green and orange domains, has the same crystal structure as the β -crystal, and its b-axis is parallel to the s-axis.

The orange domain emits differently colored fluorescence even though it has the same crystal structure as the β -crystal. Two possible reasons for this fluorescence color difference can be proposed. First, the orange domain has high-density structural defects/disorders, which enhance STE emission compared to the β -crystal. Second, nanoscale grains of α -crystals or dimer sites, which do not affect the Raman spectra, are dispersed over the domain. The gray curve in Figure 3 shows the fluorescence spectrum of the α -crystal. The spectrum of the orange domain in the SET band region (550–750 nm) agrees with that of the α -crystal, suggesting the coexistence of α -crystals or dimer sites. Indeed, Fukushima et al. recently reported that the domains of the α -crystal coexisted in the β -crystal during the temperature-induced β -to- α phase transition of perylene crystals [36]. To determine which possibility is true, fluorescence lifetime measurements of both domains are expected to provide useful information as the lifetimes for the α - and β -crystals are different by an order of magnitude (α -crystal: ~ 100 ns, β -crystal: ~ 10 ns) [23]. These measurements will be performed in future studies. However, in this study, we focused on exploring the crystal-growth mechanism that yields heterogeneous domains. In either case, whether the orange domains have defects/disorders or contain α -crystals/dimer sites, the crystal quality of the orange domain is considered lower than that of the β -crystal, thus indicating that the growth process of the orange domain is different from that of both the β -crystal and green domains and should have a mechanism that leads to low-quality crystals.

Because hexagonal crystals have the same structure as β -crystals, it is reasonable

to assume that rhombic crystals are formed in the initial stage of the crystallization process and further grow into hexagonal crystals as the solvent evaporates. Indeed, in the high-magnification fluorescence image of the hexagonal crystal, a rhombic area slightly darker than the surrounding area is visible at the center of the crystal (Figure 2e), which is considered to be a remnant of an initially formed β -crystal. According to the Gibbs-Curie-Wulff theorem, the growth rates of crystal faces are proportional to their surface free energies [37]. For the β -crystal of perylene, the rhombic crystal face (100) has the lowest surface energy, and the four lateral faces (011) and (01-1), have approximately similar free energies [18, 38]. Therefore, the crystals tend to grow with keeping a rhombic shape if the crystal growth conditions are constant. However, in the solution evaporating on the surface, the conditions change dynamically as the solvent evaporation proceeds, possibly leading to a unique crystal growth process, which does not follow the Gibbs-Curie-Wulff theorem.

We assume the following process for the growth of the hexagonal crystals from the rhombic crystals: During the growth of the rhombic crystals by the predominant lateral face growth (Figure 5a), triangular gaps are created at the top and bottom of the crystals because of a decrease in the concentration of molecules around them (Figure 5b). Crystals are then grown in these triangular areas to fill the gaps (Figure 5c). The recovery of the concentration of molecules around the crystal by the solution flow again leads to lateral face growth (Figure 5c). When this lateral face growth, followed by gap filling, occurs repeatedly, triangular areas with multiple stripes and irregular boundaries are formed (Figures 5d and 5e). When hexagonal crystals are grown through this mechanism, the crystal quality in the triangular regions is likely to be inferior to that of the other areas, where the crystal is grown in the π -stacking direction (see Figure 1f).

To validate our hypothesis, we carefully examined the entire area of the samples using fluorescence microscopy. Because the thickness of the solution film on the surface was inhomogeneous during solvent evaporation, the evaporation process completed in some areas considerably earlier than in other areas. Fluorescence microscopy observations of these areas showed that only crystals smaller than 10 μm were formed. Despite their small size, all α -crystals are rectangular (Figure 5f). However, many of the β -crystals are hexagonal with defects at the top and bottom (Figures 5g-i), similar to the shapes illustrated in Figures 5b and 5d. We believe that these crystals were formed by the quenching of crystal growth in the early stage of the lateral face/gap filling growth cycle upon the completion of solvent evaporation. The results strongly supported our hypothesis.

Conclusions

Hexagonal single crystals of perylene were grown via solution evaporation on a glass substrate by tuning and controlling the conditions influencing the crystallization process. Fluorescence microscopy revealed that the hexagonal crystals contained two triangular domains with fluorescence colors different from those in other areas of the crystals. The triangular domains emitted orange fluorescence, whereas the other domains emitted green fluorescence. Polarized ULF Raman microscopy revealed that both the orange and green domains had the same crystal structure as a β -crystal. We concluded that the difference in the fluorescence color could be attributed to the difference in the crystal quality. We propose that hexagonal crystals are formed by further growth of rhombic β -crystals as the solvent evaporates. Our results indicate that solution evaporation under tuned and controlled conditions can induce unique crystallization processes, and is a promising

technique for synthesizing organic crystals with new functionalities.

Declaration of Competing Interest

The authors declare that there is no conflict of interest.

Acknowledgments

This study was supported by the JSPS KAKENHI grant [21K05045].

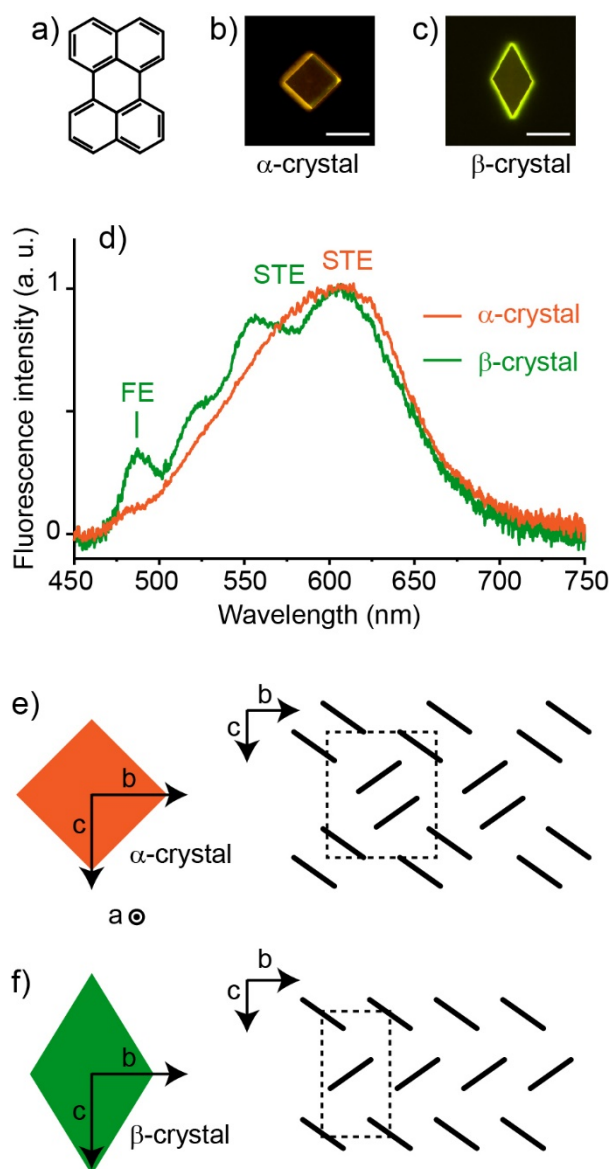


Figure 1 (a) Chemical structure of perylene. Fluorescence microscope images of (b) α -crystal and (b) β -crystal. Scale bar: 10 μ m. (d) Spatially resolved fluorescence spectra of α -crystal (orange curve) and β -crystal (green curve) measured at their central positions. FE: free exciton. STE: self-trapped exciton. (e) Schematic illustrations of α -crystal (left panel) and its crystal structure (right panel). Dotted lines represent the unit cell. (f) Schematic illustrations of β -crystal (left panel) and its crystal structure (right panel). Dotted lines represent the unit cell.

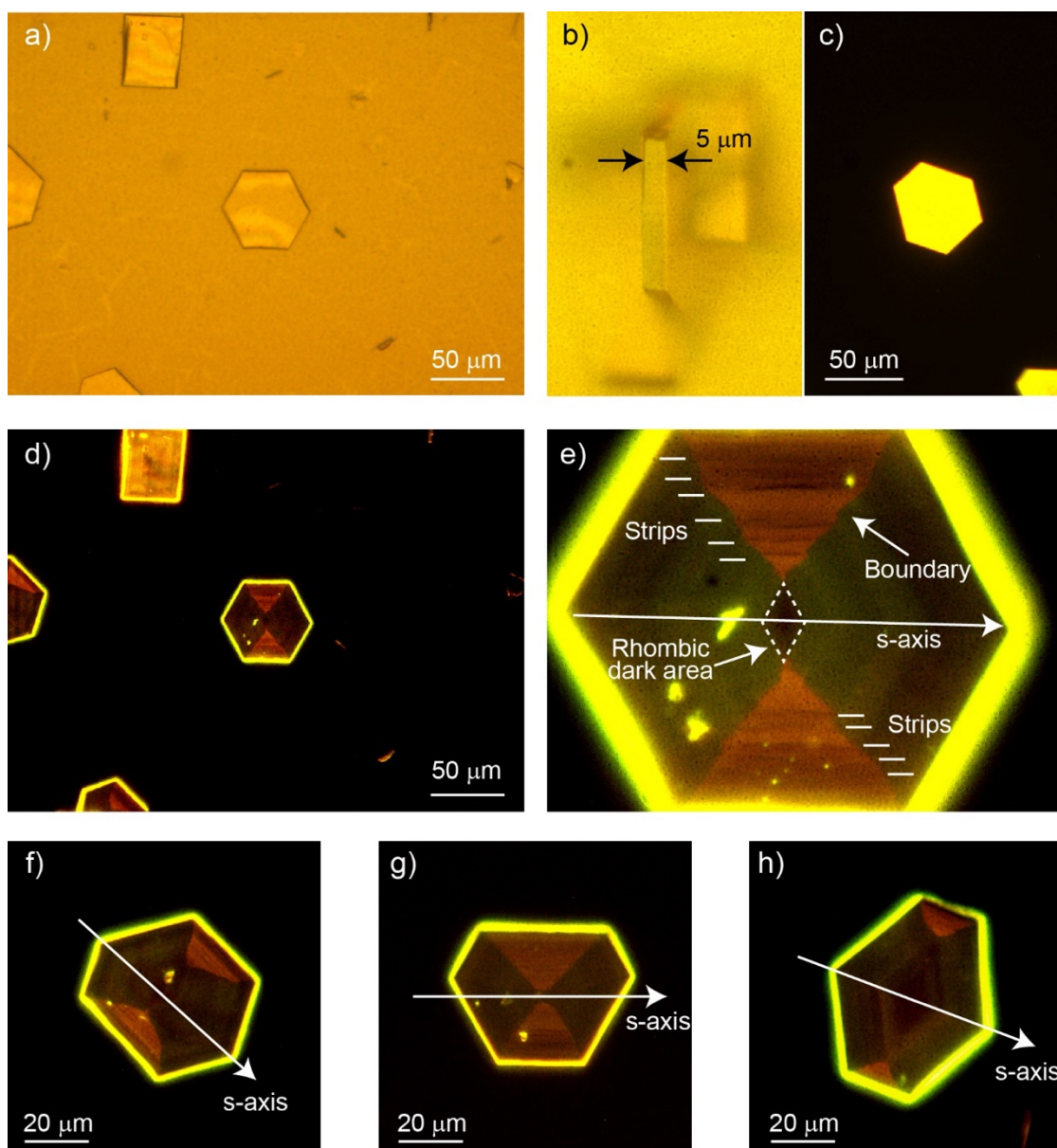


Figure 2 (a) Optical micrograph of a hexagonal crystal. (b) Side view of a hexagonal crystal. (c) Cross-polarized microscope image of a hexagonal crystal, showing the uniform color. (d) Fluorescence microscope image of the hexagonal crystal shown in (a), exhibiting patterned heterogeneous domains. (e) High-magnification fluorescence microscope image of the hexagonal crystal. The horizontal arrow shows the s-axis (see the text). (f–h) Fluorescence microscope images of distorted and elongated hexagonal crystals.

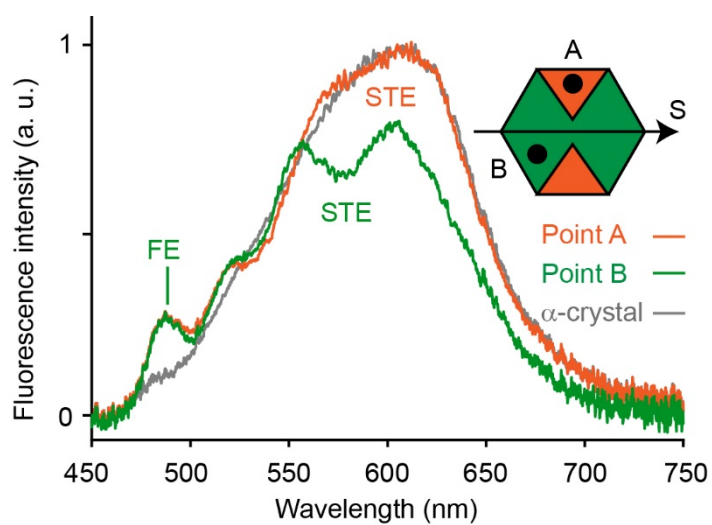


Figure 3 Spatially resolved fluorescence spectra at point A in the orange domain (orange curve) and at point B in the green domain (green curve), and fluorescence spectrum of the α -crystal (gray curve). FE: free exciton. STE: self-trapped exciton. Inset: Schematic illustration of the hexagonal crystal. Black circles indicate the positions of points A and B.

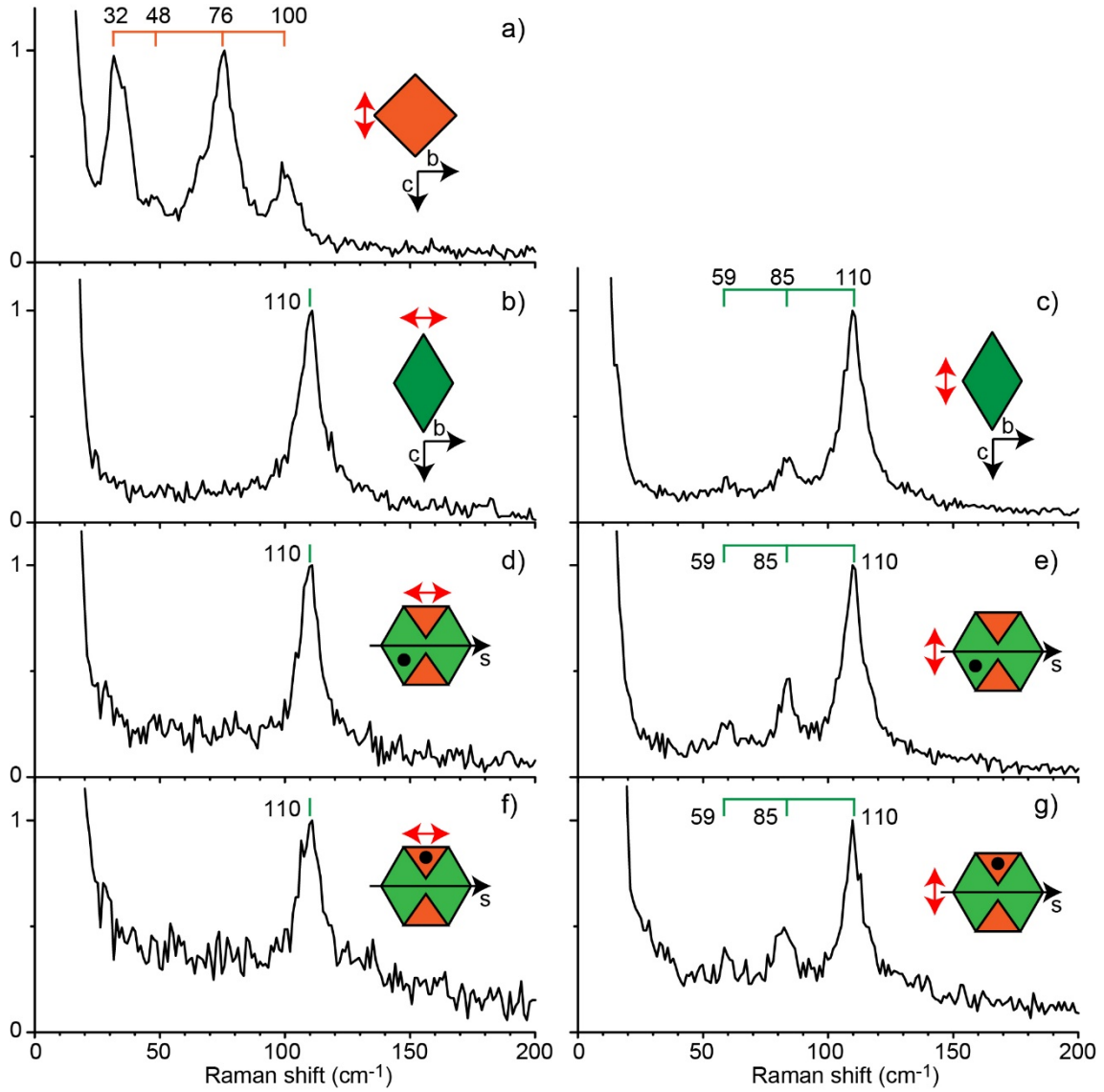


Figure 4 (a) Polarized ULF Raman spectrum of the α -crystal. Red arrow in the inset shows the polarization direction of the excitation laser. (b, c) Spectra of the β -crystal measured with two orthogonal polarizations. (d, e) Spectra at a green domain of a hexagonal crystal measured with two orthogonal polarizations. Inset: Schematic illustration of the hexagonal crystal. Black circles indicate the measured positions. (f, g) Spectra at a red domain of the hexagonal crystal measured with two orthogonal polarizations.

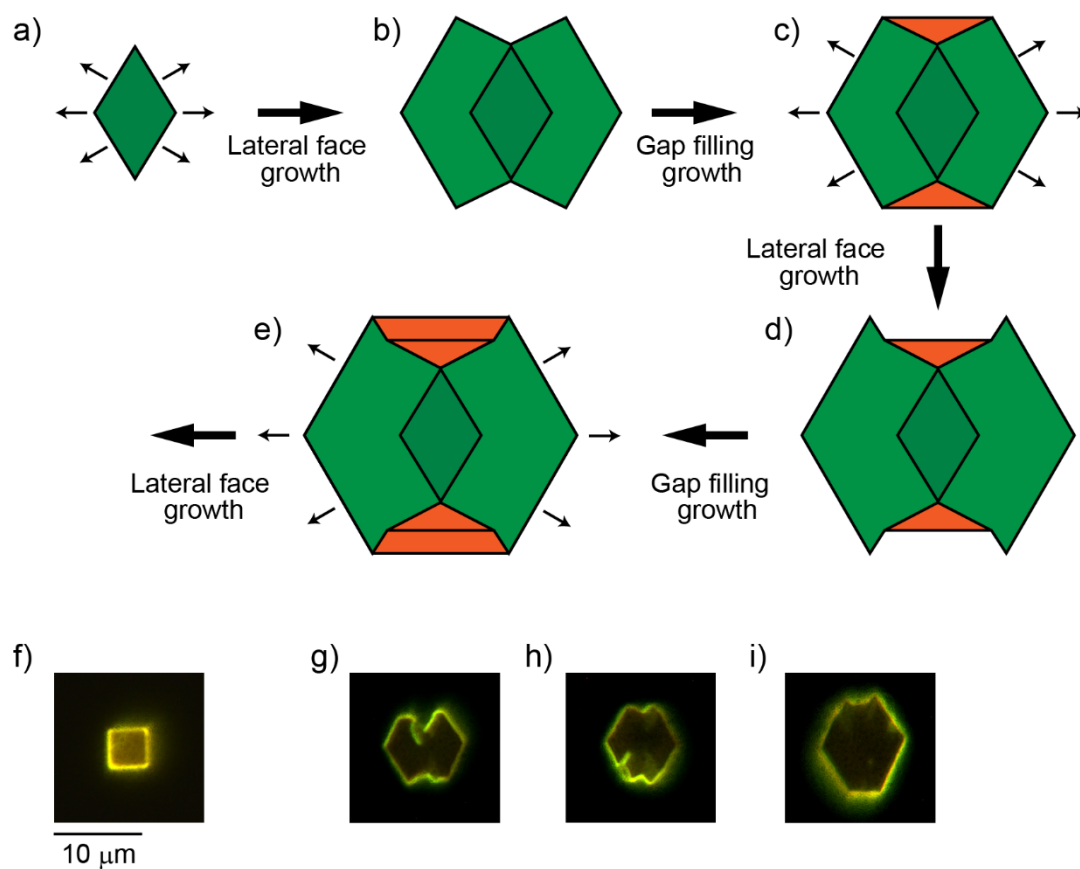


Figure 5 (a) Rhombic β -crystal formed at the initial stage of the crystallization. Arrows indicate the growth direction of the lateral faces. (b) Crystal with triangle gaps. (c) Hexagonal crystal formed after gap-filling. (d) Crystal grown from the hexagonal crystal by the lateral face growth. (e) Hexagonal crystal formed after gap-filling, showing horizontal stripes in the orange domains. (f) Small α -crystal. (g)–(i) Small β -crystals with defects.

Appendix A. Supplementary data

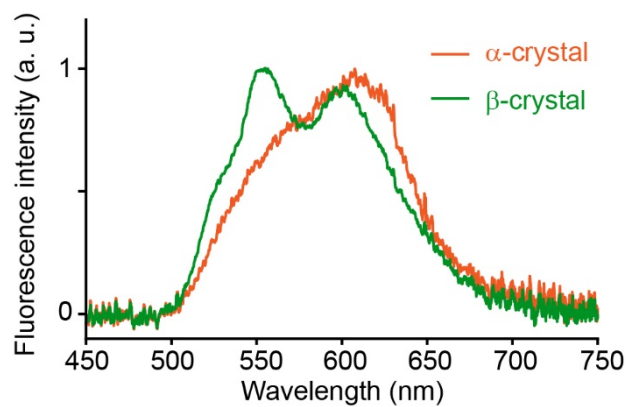


Figure S1 Fluorescence spectra of α -crystal (orange curve) and β -crystal (green curve) measured by collecting fluorescence from the entire crystals.

References

- [1] H. E. Katz,
Recent advances in semiconductor performance and printing processes for
organic transistor-based electronics,
Chem. Mater., 16 (2004), pp. 4748–4756.
<https://doi.org/10.1021/cm049781j>
- [2] M. O'Neill, S. M. Kelly,
Ordered materials for organic electronics and photonics,
Adv. Mater., 23 (2011), pp. 566–584.
<https://doi.org/10.1002/adma.201002884>
- [3] D. L. Mitchell, S. B. Lee, L. Trofin, N. Li, T. K. Nevanen, H. Söderlund, C. R.
Martin,
Smart nanotubes for bioseparations and biocatalysis,
J. Am. Chem. Soc., 124 (2002), pp. 11864–11865.
<https://doi.org/10.1021/ja027247b>
- [4] Z. Song, H. Zhou,
Towards sustainable and versatile energy storage devices: an overview of
organic electrode materials,
Energy Environ. Sci., 6 (2013), pp. 2280–2301.
<https://doi.org/10.1039/C3EE40709H>
- [5] Y. Diao, L. Shaw, Z. Bao, S. C. Mannsfeld,
Morphology control strategies for solution-processed organic semiconductor
thin films,
Energy & Environ. Sci., 7 (2014), pp. 2145–2159.

<https://doi.org/10.1039/c4ee00688g>

- [6] A. P. Schenning, F. B. Benneker, H. P. Geurts, X. Y. Liu, R. J. Nolte, Porphyrin wheels, *J. Am. Chem. Soc.*, 118 (1996), pp. 8549–8552.
<https://doi.org/10.1021/ja961234e>
- [7] K. Takazawa, Micrometer-sized rings self-assembled from thiacyanine dye molecules and their waveguiding properties, *Chem. Mater.*, 19 (2007), pp. 5293–5301.
<https://doi.org/10.1021/cm071762x>
- [8] M. Kotani, K. Kakinuma, M. Yoshimura, K. Ishii, S. Yamazaki, T. Kobori, H. Okuyama, H. Kobayashi, H. Tada, Charge carrier transport in high purity perylene single crystal studied by time-of-flight measurements and through field effect transistor characteristics, *Chem. Phys.*, 325 (2006), pp. 160–169.
<https://doi.org/10.1016/j.chemphys.2006.02.017>
- [9] J. W. Lee, H. S. Kang, M. K. Kim, K. Kim, M. Y. Cho, Y. W. Kwon, J. Joo, J. I. Kim, C. S. Hong, Electrical characteristics of organic perylene single-crystal-based field-effect transistors, *J. Appl. Phys.*, 102 (2007), pp. 124104.
<https://doi.org/10.1063/1.2822453>
- [10] A. S. Molinari, H. Alves, Z. Chen, A. Facchetti, A. F. Morpurgo, High electron mobility in vacuum and ambient for PDIF-CN₂ single-crystal

- transistors,
J. Am. Chem. Soc., 131 (2009), pp. 2462–2463.
<https://doi.org/10.1021/ja809848y>
- [11] R. T. Weitz, K. Amsharov, U. Zschieschang, E. B. Villas, D. K. Goswami, M. Burghard, H. Dosch, M. Jansen, K. Kern, H. Klauk,
 Organic n-channel transistors based on core-cyanated perylene carboxylic diimide derivatives,
J. Am. Chem. Soc., 130 (2008), pp. 4637–4645.
<https://doi.org/10.1021/ja074675e>
- [12] R. W. I. de Boer, M. E. Gershenson, A. F. Morpurgo, V. Podzorov,
 Organic single-crystal field-effect transistors,
Phys. Status Solidi A, 201 (2004), pp. 1302–1331.
<https://doi.org/10.1002/pssa.200404336>
- [13] H. Klauk,
 Organic thin-film transistors,
Chem. Soc. Rev., 39 (2010), pp. 2643–2666.
<https://doi.org/10.1039/B909902F>
- [14] A. T. Camerman, J. Trotter,
 The crystal and molecular structure of perylene,
Proc. R. Soc. Lond. A Math. Phys. Sci., 279 (1964), pp. 129–146.
<https://doi.org/10.1098/rspa.1964.0094>
- [15] J. Tanaka
 The electronic spectra of aromatic molecular crystals. II. The crystal structure and spectra of perylene,

- Bull. Chem. Soc. Jpn., 36 (1963), pp. 1237–1249.
<https://doi.org/10.1246/bcsj.36.1237>
- [16] T. Rangel, A. Rinn, S. Sharifzadeh, F. H. da Jornada, A. Pick, S. G. Louie, G. Witte, L. Kronik, J. B. Neaton, S. Chatterjee,
 Low-lying excited states in crystalline perylene,
 Proc. Natl. Acad. Sci., 115 (2018), pp. 284–289.
<https://doi.org/10.1073/pnas.1711126115>
- [17] T. Yago, Y. Tamaki, A. Furube, R. Katoh,
 Growth of β -perylene crystal,
 Chem. Lett., 36 (2007), pp. 370–371.
<https://doi.org/10.1246/cl.2007.370>
- [18] J. H. Urbelis, J. A. Swift,
 Phase-Selective Crystallization of Perylene on Monolayer Templates,
 Crys. Growth Des., 14 (2014), pp. 5244–5251.
<https://doi.org/10.1021/cg501030g>
- [19] A. Pick, M. Klues, A. Rinn, K. Harms, S. Chatterjee, G. Witte,
 Polymorph-selective preparation and structural characterization of perylene
 single crystals,
 Crys. Growth Des., 15 (2015), pp. 5495–5504.
<https://doi.org/10.1021/acs.cgd.5b01130>
- [20] T. Kobayashi,
 The observation of the excimer formation process in pyrene and perylene
 crystals using a picosecond ruby laser and streak camera,
 J. Chem. Phys., 69 (1978), pp. 3570–3574.

<https://doi.org/10.1063/1.437062>

- [21] H. Auweter, D. Ramer, B. Kunze, H.C. Wolf,
The dynamics of excimer formation in perylene crystals,
Chem. Phys. Lett., 85 (1982), pp. 325–329.
[https://doi.org/10.1016/0009-2614\(82\)80303-5](https://doi.org/10.1016/0009-2614(82)80303-5)
- [22] B. Walker, H. Port, H.C. Wolf,
The two-step excimer formation in perylene crystals,
Chem. Phys., 92 (1985), pp. 177–185.
[https://doi.org/10.1016/0301-0104\(85\)85014-X](https://doi.org/10.1016/0301-0104(85)85014-X)
- [23] H. Nishimura, T. Yamaoka, K. Mizuno, M. Iemura, A. Matsui,
Luminescence of free and self-trapped excitons in α - and β -perylene crystals,
J. Phys. Soc. Jpn., 53 (1984), pp. 3999–4008.
<https://doi.org/10.1143/JPSJ.53.3999>
- [24] T. Fujino, T. Tahara,
Femtosecond fluorescence up-conversion microscopy: exciton dynamics in α -
perylene microcrystal,
J. Phys. Chem. B, 107 (2003), pp. 5120–5122.
<https://doi.org/10.1021/jp034037s>
- [25] A. Furube, M. Murai, Y. Tamaki, S. Watanabe, R. Katoh,
Effect of aggregation on the excited-state electronic structure of perylene
studied by transient absorption spectroscopy,
J. Phys. Chem. A, 110 (2006), pp. 6465–6471.
<https://doi.org/10.1021/jp060649b>
- [26] T. Yago, Y. Tamaki, A. Furube, R. Katoh,

- Self-trapping limited exciton diffusion in a monomeric perylene crystal as revealed by femtosecond transient absorption microscopy, *Phys. Chem. Chem. Phys.*, 10 (2008), pp. 4435–4441.
<https://doi.org/10.1039/B801856A>
- [27] X. Wang, Q. Liao, Q. Kong, Y. Zhang, Z. Xu, X. Lu, H. Fu, Whispering-Gallery-Mode Microlaser Based on Self-Assembled Organic Single-Crystalline Hexagonal Microdisks, *Angew. Chem. Int. Ed.*, 53 (2014), pp. 5863–5867.
<https://doi.org/10.1002/anie.201310659>
- [28] K. Takazawa, Understanding the emission pattern produced by focused laser beam excitation of perylene square single crystals, *Chem. Phys. Lett.*, 667, (2017) pp. 284–289.
<https://doi.org/10.1016/j.cplett.2016.10.083>
- [29] K. Takazawa, Y. Kitahama, Y. Kimura, G. Kido, Optical waveguide self-assembled from organic dye molecules in solution, *Nano Lett.*, 5 (2005), pp. 1293–1296.
<https://doi.org/10.1021/nl050469y>
- [30] K. Sato, R. Katoh, Fluorescence properties of β -perylene crystals prepared by a physical vapor transport method under atmospheric pressure, *Chem. Phys. Lett.*, 730, (2019) pp. 312–315.
<https://doi.org/10.1016/j.cplett.2019.06.031>
- [31] M. Botoshansky, F. H. Herbstein, M. Kapon,

- Towards a complete description of a polymorphic crystal: The example of perylene: Redetermination of the structures of the (Z= 2 and 4) polymorphs, *Helv. Chim. Acta*, 86 (2003), pp. 1113–1128.
<https://doi.org/10.1002/hlca.200390097>
- [32] K. Takazawa, J. I. Inoue, K. Mitsuishi, T. Takamasu,
 Micrometer-Scale Photonic Circuit Components Based on Propagation of Exciton Polaritons in Organic Dye Nanofibers,
Adv. Mater., 23 (2011), pp. 3659–3663.
<https://doi.org/10.1002/adma.201100827>
- [33] M. Suzuki, T. Yokoyama, M. Ito,
 Polarized Raman spectra of naphthalene and anthracene single crystals,
Spectrochim. Acta A Mol. Spectrosc., 24 (1968), pp. 1091–1107.
[https://doi.org/10.1016/0584-8539\(68\)80129-1](https://doi.org/10.1016/0584-8539(68)80129-1)
- [34] A. Fruhling,
 Low Frequency Raman Spectrum of a Benzene Single Crystal,
J. Chem. Phys., 18 (1950), pp. 1119–1119.
<https://doi.org/10.1063/1.1747883>
- [35] T. J. Kosic, C. L. Schosser, D. D. Dlott,
 Vibrational spectroscopy of solid state molecular dimers,
Chem. Phys. Lett., 96 (1983), pp. 57–64.
[https://doi.org/10.1016/0009-2614\(83\)80117-1](https://doi.org/10.1016/0009-2614(83)80117-1)
- [36] M. Fukushima, K. Sato, Y. Fujimoto, F. Ito, R. Katoh
 Observation of an Intermediate State in the Solid–Solid Phase Transition of a Single Crystal of Perylene,

Cryst. Growth Des. 2022, 22, 4, pp. 2071–2075

<https://doi.org/10.1021/acs.cgd.2c00015>

[37] R. Li, X. Zhang, H. Dong, Q. Li, Z. Shuai, W. Hu,

Gibbs–Curie–Wulff theorem in organic materials: a case study on the relationship between surface energy and crystal growth,

Adv. Mater., 28 (2016), pp. 1697–1702.

<https://doi.org/10.1002/adma.201504370>

[38] Z. Z. Li, L. S. Liao, X. D. Wang,

Controllable synthesis of organic microcrystals with tunable emission color and morphology based on molecular packing mode.

Small, 14 (2018), pp. 1702952.

<https://doi.org/10.1002/sml.201702952>